

Sign structure in the square-lattice t - t' - J model and numerical consequences

Xin Lu,^{1,*} Jia-Xin Zhang,^{2,*} Shou-Shu Gong,^{3,†} D. N. Sheng,^{4,‡} and Zheng-Yu Weng^{2,§}

¹*School of Physics, Beihang University, Beijing 100191, China*

²*Institute for Advanced Study, Tsinghua University, Beijing 100084, China*

³*School of Physical Sciences, Great Bay University, Dongguan 523000, China, and
Great Bay Institute for Advanced Study, Dongguan 523000, China*

⁴*Department of Physics and Astronomy, California State University, Northridge, California 91330, USA*

Understanding the doped Mott insulator is a central challenge in condensed matter physics. This study identifies an intrinsic Berry-phase-like sign structure for the square-lattice t - t' - J model with the nearest-neighbor (t) and next-nearest-neighbor hopping (t'), which could help explain the origin of the quasi-long-range superconducting and stripe phases observed through density matrix renormalization group (DMRG) calculation. We first demonstrate that the hole binding underlies both the superconducting and stripe orders, and then show that the hole pairing generically disappears once the phase-string or mutual statistics component of the sign structure is switched off in DMRG calculation. In the latter case, the superexchange interaction no longer plays a crucial role in shaping the charge dynamics, where a Fermi-liquid-like phase with small hole Fermi pockets is found. It is in sharp contrast to the large Fermi surfaces in either the stripe phase found at $t'/t < 0$ or the superconducting phase at $t'/t > 0$ in the original t - t' - J model on 6-leg ladder. Our results shed new light on the origin of hole binding as well as the interplay between superconductivity and charge order in doped Mott insulators.

Introduction.— Understanding the emergence of unconventional superconductivity (SC) and its pairing mechanism is a major task in condensed matter physics [1, 2]. Since the unconventional SC is usually realized by doping the parent Mott insulators, the Hubbard and effective t - J models are commonly taken as the minimal models to study SC in doped Mott insulators [1–8]. While analytical solutions for two-dimensional correlated systems may be still not well controlled, numerical calculations have found different quantum phases in the doped square-lattice Hubbard and t - J models [9–43]. In particular, for quasi-1D systems some phases have been established, including the spin and charge intertwined charge density wave (CDW) order with relatively weak SC correlation [9–23], as well as the Luther-Emery liquid with coexistent quasi-long-range SC and CDW orders [44, 45] by turning on the next-nearest-neighbor (NNN) hopping t' with both positive and negative t'/t (t is the nearest-neighbor (NN) hopping) [29–33].

Towards wider systems, recent density matrix renormalization group (DMRG) studies on 6-leg t - t' - J model [34–39] find that while the CDW phase persists at $t'/t < 0$ near the optimal doping [34, 35], it gives way to a robust d -wave SC phase with tuning $t'/t > 0$ [35–38]. The Fermi surface topology results [35, 37] indicate that this SC phase may provide a natural understanding on the cuprates with electron doping, and the $t'/t < 0$ side should correspond to the hole doping [46–48], thus leaving the emergent SC at hole-doped cuprates still puzzling. On the other hand, DMRG results suggest that hole binding may also exist in the CDW phase [35]. These significant numerical results naturally raise several important questions such as what is the origin of hole binding? Whether the holes are indeed paired in the CDW phase, and if they are, what leads to the different SC and CDW phases?

In this work, combined with the state-of-the-art DMRG calculations, we demonstrate that in the 6-leg t - t' - J model near the optimal doping, the hole binding underlies both the SC

and CDW phases as a common feature either on the $t'/t < 0$ or $t'/t \geq 0$ side. Meanwhile, by analytical analyses we identify a phase-string in this model as the mutual-statistical sign structure [49–51], and by switching off this phase-string we show that the hole binding is diminished, and both the stripe and SC phases are transited to a Fermi-liquid-like (FL-like) state [52]. Correspondingly, the original large Fermi surfaces are reduced to the small Fermi pockets in the absence of the phase-string that characterizes the many-body quantum entanglement between the spin and charge degrees of freedom. Our findings demonstrate an entirely new mechanism, based on the phase string, for hole binding in the SC and CDW phases, which also provides an understanding on the competition between SC and CDW with tuning t'/t , and will be inspirational in constructing the microscopic description of novel states in doped Mott insulators.

Exact sign structure of the t - t' - J model.— We first discuss the sign structure in the t - t' - J model, which is defined as $H_{t-t'-J} = H_{t-t'} + H_J$, with both the NN $\langle ij \rangle$ and NNN $\langle\langle ij \rangle\rangle$ hopping terms

$$H_{t-t'} \equiv -t \sum_{\langle ij \rangle \sigma} c_{i,\sigma}^\dagger c_{j,\sigma} - t' \sum_{\langle\langle ij \rangle\rangle \sigma} c_{i,\sigma}^\dagger c_{j,\sigma} + \text{h.c.}, \quad (1)$$

as well as the NN superexchange term $H_J = J \sum_{\langle ij \rangle} (\mathbf{S}_i \cdot \mathbf{S}_j - \frac{1}{4} n_i n_j)$, where $c_{i,\sigma}^\dagger$ and $c_{i,\sigma}$ are the creation and annihilation operators for the electron with spin $\sigma/2$ ($\sigma = \pm 1$) at the site i , \mathbf{S}_i is the spin-1/2 operator, and $n_i \equiv \sum_{\sigma} c_{i,\sigma}^\dagger c_{i,\sigma}$ is the electron number operator.

The central theme to be established in this work is that the physics of the t - t' - J model is essentially dictated by the sign structure of the model just like that a FL state is determined by the Fermi sign structure (statistics) in a conventional weakly interacting system. Here the sign structure refers to the sign factor τ_C in the following partition function for the system at

a finite hole doping

$$Z_{t-t'-J} \equiv \text{Tr} e^{-\beta H_{t-t'-J}} = \sum_C \tau_C W_{t-t'-J}[C], \quad (2)$$

where β is the inverse temperature, $W_{t-t'-J}[C] \geq 0$ denotes the positive weight for each closed loop C of all spin-hole coordinates on the square lattice, and a quantum sign associated with the path C is characterized by $\tau_C = \pm 1$. Here both W and τ may be generally determined via the stochastic series expansion (cf. Sec. I of the Supplemental Materials (SM) [53]):

$$Z_{t-t'-J} = \sum_{n=0}^{\infty} \sum_{\{\alpha_i\}} \frac{\beta^n}{n!} \prod_{i=0}^{n-1} \langle \alpha_i | (-H_{t-t'-J}) | \alpha_{i+1} \rangle, \quad (3)$$

where for each n , $|\alpha_n\rangle = |\alpha_0\rangle$ denoting the many-body hole and spin-Ising bases (with \hat{z} as the quantization axis) such that the partition function is characterized by a series of closed loops of step n 's, denoted by C , which include both hopping and superexchange processes. The total sign collected by τ_C is precisely given by [53]

$$\tau_C \equiv \tau_C^0 \times (-1)^{N_{\downarrow}^h} \quad (4)$$

with $\tau_C^0 \equiv (-1)^{N_{\text{ex}}^h} \times [\text{sgn}(t')]^{N_{t'}^h}$, in which N_{ex}^h denotes the total number of exchanges between the identical holes, i.e., the usual Fermi statistical sign structure of the doped holes like in a semiconductor, and $N_{t'}^h$ counts the total steps of the NNN hopping of the holes in the path C , resulting in a geometric Berry phase at $t' < 0$. In Eq. (4), the NN hopping integral is assumed to be always positive for simplicity, i.e., $t > 0$.

The sign factor $(-1)^{N_{\downarrow}^h}$ in Eq. (4) is known as the phase-string [49–51], in which N_{\downarrow}^h denotes the total mutual exchanges between the holes and down-spins at the NN hoppings, which has been identified in the t - J model at $t' = 0$ [51] as a novel long-range entanglement or mutual statistics between the doped holes and the spins [6, 50]. The phase-string Berry phase is thus generally present in the t - t' - J model. To explicitly see its effect, we point out that if the hopping term $H_{t-t'}$ is changed to

$$H_{\sigma t-t'} \equiv -t \sum_{\langle ij \rangle_{\sigma}} \sigma c_{i,\sigma}^{\dagger} c_{j,\sigma} - t' \sum_{\langle\langle ij \rangle\rangle_{\sigma}} c_{i,\sigma}^{\dagger} c_{j,\sigma} + \text{h.c.}, \quad (5)$$

with the superexchange term H_J unchanged, which is to be called the σt - t' - J model below, the τ_C in Eq. (4) will reduce to the sole sign structure in the partition function [53]

$$Z_{\sigma t-t'-J} = \sum_C \tau_C^0 W_{t-t'-J}[C]. \quad (6)$$

In other words, one can precisely switch off the phase-string in the σt - t' - J model such that the sign structure becomes a conventional τ_C^0 with the same amplitude $W_{t-t'-J}[C]$ [53]. The above sign structures for both models are exact at any finite size, arbitrary doping, and temperature.

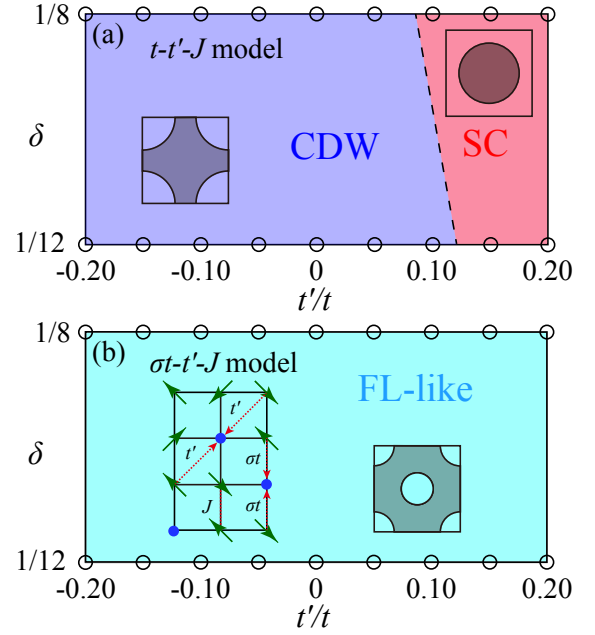


FIG. 1. Phase diagrams of the t - t' - J model (a) and σt - t' - J model (b), determined on the $L_y = 6$ cylinder. At the range of $-0.2 \leq t'/t \leq 0.2$ and doping level $1/12 \leq \delta \leq 1/8$, the CDW and SC phases present in the t - t' - J model are replaced by a ubiquitous FL-like state in the σt - t' - J model. The topology of large Fermi surfaces in the CDW and SC phases in (a) are reduced to that of small hole pockets in the FL-like phase in (b), as illustrated by the cartoon plots of the momentum distribution (the darker regions indicate the electron occupancy with higher probability). Here the σt - t' - J model is distinct from the t - t' - J model only by a spin-dependent sign in the NN hopping integral σt with the same NNN hopping t' and NN superexchange J , as indicated in the left inset of (b) with the arrows (circles) denoting electrons (holes). Following Ref. [37], the phase boundary in the t - t' - J model is determined by examining charge density profile and comparing different correlation functions.

Phase diagrams obtained from DMRG.— In the following, we shall accurately determine the ground states of both models using DMRG calculations [54] to reveal the important role played by the phase-string component of the sign structure in hole pairing. We choose $t/J = 3$ to mimic a large Hubbard $U/t = 12$ and tune the hopping ratio in the region of $-0.2 \leq t'/t \leq 0.2$. We focus on two doping levels at $\delta = N_h/N = 1/12$ and $1/8$, where N_h is the hole number and N is the total site number. We study the models on cylinder geometry with the periodic boundary condition along the circumference direction (y) and open boundary along the axis direction (x), and use L_y and L_x to denote the site numbers along the two directions, respectively. For the t - t' - J model with spin SU(2) symmetry, we keep the bond dimensions up to 12000 SU(2) multiplets [55] (equivalent to about 36000 U(1) states). For the σt - t' - J model, we use the U(1) symmetry and keep the bond dimensions up to 15000 states. We obtain accurate local measurements and correlation functions on the $L_y = 4, 6$ cylinders with the truncation error near 1×10^{-6} .

We illustrate the phase diagrams obtained on 6-leg cylinder

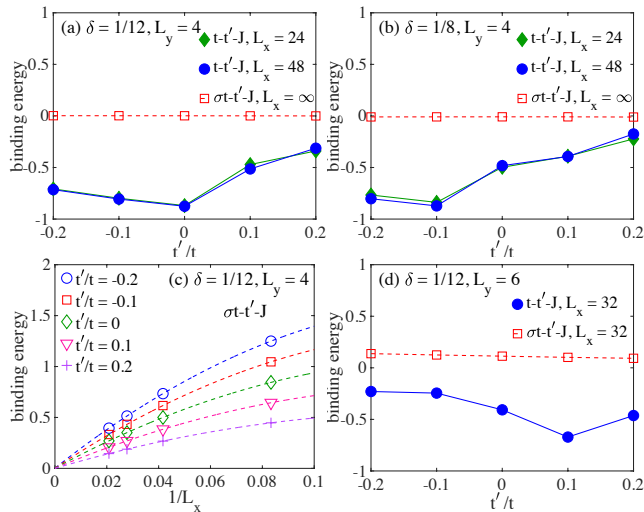


FIG. 2. Binding energy in the $t-t'-J$ and $\sigma t-t'-J$ models. (a) and (b) show the binding energies on the 4-leg cylinders at $\delta = 1/12$ and $\delta = 1/8$, respectively. The results of the $t-t'-J$ and $\sigma t-t'-J$ models are marked with solid and open symbols, respectively. We present two sizes ($L_x = 24$ and 48) for the $t-t'-J$ model to show the good convergence of the binding energy with L_x . For the $\sigma t-t'-J$ model, the binding energies exhibit a pronounced finite-size effect, and we show the results after the size extrapolation to the infinite- L_x limit. (c) Extrapolations of binding energies versus system length for the 4-leg $\sigma t-t'-J$ model at $\delta = 1/12$, which are fitted by a second-order polynomial function $\mathcal{C}(1/L_x) = \mathcal{C}(0) + a/L_x + b/L_x^2$. (d) Binding energies for the two models on the $L_y = 6, L_x = 32$ cylinder at $\delta = 1/12$. The results of the $\sigma t-t'-J$ model are obtained using 12000 bond dimensions. For the $t-t'-J$ model, the binding energies are calculated using the energies $E(N_h, S)$ after the extrapolation to the infinite-bond-dimension limit (see SM Sec. II [53]).

in Fig. 1. With the phase-string, the $t-t'-J$ model shows the CDW and SC phases as a function of t'/t [Fig. 1(a)], both of which have large Fermi surfaces. By contrast, by switching off the phase-string, the $\sigma t-t'-J$ model exhibits a FL-like phase with small Fermi pockets in the whole studied range of t'/t [Fig. 1(b)], which is dictated by the Fermi signs in τ_C^0 .

Binding energy.— An important result we find in this work is that in the $t-t'-J$ model the holes form pairs not only in the SC phase, but also in the CDW phase. Following the usual definition, we calculate the binding energy E_b as

$$E_b \equiv E(N_h, 0) + E(N_h - 2, 0) - 2E(N_h - 1, 1/2), \quad (7)$$

where $E(N_h, S)$ denotes the lowest-energy in the sector with hole number N_h and total spin quantum number S (total spin- z component S) for the $t-t'-J$ ($\sigma t-t'-J$) model. The negative E_b characterizes hole binding. On the 4-leg cylinder, we obtain well converged binding energy. In the $t-t'-J$ model, although the system can exhibit different phases with tuning parameters [32], the binding energies, which converge quickly with system length, are always negative [Figs. 2(a) and 2(b)]. On the other hand, for the $\sigma t-t'-J$ model, the binding energies are positive and strongly size dependent, which are clearly extrapolated to zero for $L_x \rightarrow \infty$ [Fig. 2(c) and see SM Sec.

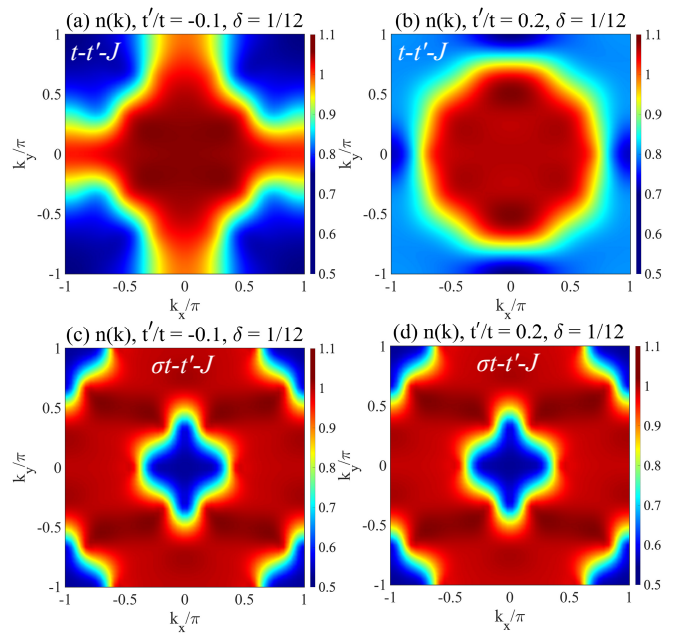


FIG. 3. Electron distribution in the momentum space $n(\mathbf{k})$ on 6-leg cylinder with $\delta = 1/12$. (a) and (b) show the results of the $t-t'-J$ model with a large Fermi surface. The Fermi surface topology is different in the CDW and SC phases. (c) and (d) show the results of $\sigma t-t'-J$ model. The electrons of spin-up and spin-down in $n(\mathbf{k})$ are displaced by (π, π) .

II [53] for the binding energy scaling at $\delta = 1/8$).

To explore the binding energy towards two dimensions, we also calculate the binding energy on the $L_y = 6$ cylinder as presented in Fig. 2(d), showing qualitatively the same conclusion. Furthermore, the similar result is also found on the 5-leg systems (SM Sec. II [53]), suggesting the hole binding as a universal feature on both even- and odd-leg systems at finite doping. For computing the binding energy in the $t-t'-J$ model, the energies $E(N_h, S)$ in Eq. (7) have all been extrapolated to the infinite-bond-dimension limit (SM Sec. II [53]). For the $\sigma t-t'-J$ model, the obtained binding energies, which are almost independent of the kept bond dimension, have small positive values around 0.1, much smaller than the values for the same L_x on the 4-leg cylinder. Remarkably, while the pairing correlation decays exponentially in the CDW phase of the 6-leg $t-t'-J$ model [Fig. 4(c)], the hole pairing still exists, which is quite consistent with the characteristic of a pseudo-gap phase [6]. Next, we will further discuss this point from the perspective of correlation functions. Our results show that the hole pairing is indeed diminished no matter in what phase if one switches off the phase-string precisely.

Fermi surface.— The electron momentum distributions, $n(\mathbf{k}) = \frac{1}{N} \sum_{i,j,\sigma} \langle \hat{c}_{i,\sigma}^\dagger \hat{c}_{j,\sigma} \rangle e^{i\mathbf{k} \cdot (\mathbf{r}_i - \mathbf{r}_j)}$, are demonstrated in Fig. 3. The $t-t'-J$ model always exhibits a large Fermi surface with hole binding as given above, but the topology of Fermi surface has a strong t'/t dependence. By contrast, the $\sigma t-t'-J$ model shows two small Fermi pockets at $\mathbf{k} = (\pi, \pi)$ and $(0, 0)$, which have a weak t'/t dependence and are contributed

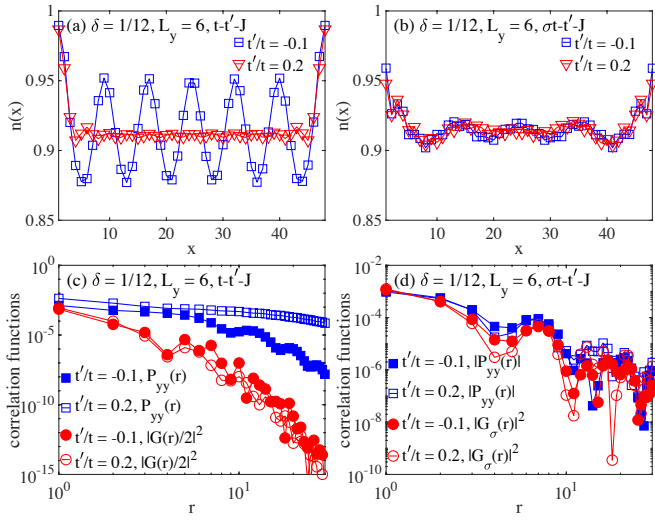


FIG. 4. Charge density profile and correlation functions on the 6-leg cylinder with $L_x = 48$ and $\delta = 1/12$. (a) and (b) show the charge density profiles $n(x)$ for the t - t' - J and σt - t' - J models, respectively. (c) and (d) are the double logarithmic plots of the pairing correlation $P_{yy}(r)$ and single-particle Green's function $G(r)$ for the t - t' - J and σt - t' - J models. Note that we only show the σ component of the single-particle Green's function in the σt - t' - J model, due to the absence of spin $SU(2)$ symmetry [52]. The results of more correlation functions and the fitted decay exponents are summarized in Table I.

from the spin-up and spin-down propagators, respectively (see SM Sec. IV for the results of other parameters [53]). For both spin components, the quasi-long-range single-particle correlations $G_\sigma(r) \equiv \langle c_{(x,y),\sigma}^\dagger c_{(x+r,y),\sigma} \rangle \sim r^{-K_G}$ with $K_G \approx 1$ [Fig. 4(d)] resemble a FL-like state, which smoothly persists to a finite t'/t (cf. Table I). Such a non-pairing state, which has been reported at $t'/t = 0$ in the 2-leg and 4-leg systems [52], appears to be insensitive to t'/t and stable on larger system size.

CDW profile and correlation functions.— Next, we characterize the two systems through charge density profile and correlation functions. We measure the average charge density distribution in the column x as $n(x) = \sum_{y=1}^{L_y} \langle \hat{n}(x, y) \rangle / L_y$. For the t - t' - J model on 6-leg cylinder, one can see a clear charge density oscillation with a period of $4/(L_y \delta)$ in the CDW phase and uniform charge distribution in the SC phase [Fig. 4(a)]. On the other hand, the charge density distribution has no apparent dependence on t'/t in the σt - t' - J model, and the charge oscillation is quite weak and without a well-defined periodicity by switching off the phase-string [Fig. 4(b)].

We further compare different correlation functions. We examine the spin-singlet pairing correlation between the vertical bonds $P_{y,y}(r) \equiv \langle \Delta_y^\dagger(x, y) \Delta_y(x+r, y) \rangle$, where the pairing operator is defined for two NN sites (x, y) and $(x, y+1)$, i.e. $\Delta_y(x, y) = (c_{(x,y),\uparrow} c_{(x,y+1),\downarrow} - c_{(x,y),\downarrow} c_{(x,y+1),\uparrow}) / \sqrt{2}$. In the t - t' - J model [Fig. 4(c)], the pairing correlation decays algebraically with strong magnitudes in the SC phase but is suppressed to decay exponentially in the CDW phase. Remarkably, the weakened pairing correlation in the CDW phase is

still much stronger than two single-particle correlator $G^2(r)$, which could be consistent with a pseudogap phase with hole binding but lacking phase coherence due to the strong CDW. Such pseudogap-like behaviors have also been observed in the triangular-lattice t - J model [56], which also sits near a SC phase and may be common in doped Mott insulators.

For the σt - t' - J model, we find that all the correlations exhibit a nice algebraic decay (see Fig. 4(d) and Table I), and the correlations behave smoothly and consistently as a function of t'/t by switching off the phase-string. The pairing correlation behaving as $G^2(r)$ [Fig. 4(d)] agrees with the prediction of a FL-like state and confirms no quasi-long-range SC order. Our results indicate no phase transition in the σt - t' - J model and only a FL-like phase exists. In particular, the quasi-long-ranged Green's function with $K_G \approx 1.0$ is consistent with the description of the Landau Fermi liquid theory.

Conclusion.— By using DMRG calculation, we have unveiled that the hole pairs constitute the basic building blocks not only in the SC but also in the CDW phase of the t - t' - J model. We have also identified the precise sign structure of the doped holes, a geometric Berry phase depending on the sign of t' , and the phase-string mutual statistics between charge and spin degrees of freedom. In particular, a mere geometric Berry phase at $t' < 0$, with the same amplitude $W_{t-t'-J}[C]$ [cf. Eqs. (2) and (4)], may stabilize the stripe over SC order for 6-leg cylinders. By turning off the phase-string, the hole pairing gets diminished to result in a FL-like phase with no more SC and stripe orders, and the corresponding Fermi surface also drastically reconstructs to become small pockets. This FL-like phase is no longer sensitive to the sign of t' . The phase-string brings in a strong correlation effect that is responsible for not only the hole pairing [57, 58] but also restoring a large Fermi surface via “momentum shifting” [59–61]. Namely the one-to-one correspondence principle of the Landau paradigm, which works for weak interaction in the conventional FL/BCS description, is generally violated here.

Acknowledgments.— We acknowledge stimulating discussions with Zheng Zhu and Hong-Chen Jiang. X. L. and S. S. G. were supported by the National Natural Science Foundation of China (Grants No. 12274014 and No. 11834014). J. X. Z. and Z. Y. W. were supported by MOST of China (Grant No. 2017YFA0302902). D. N. S. was supported by the US National Science Foundation Grant No. PHY-2216774.

* Both authors contributed equally to this work.

† shoushu.gong@gbu.edu.cn

‡ donna.sheng1@csun.edu

§ weng@mail.tsinghua.edu.cn

[1] B. Keimer, S. A. Kivelson, M. R. Norman, S. Uchida, and J. Zaanen, *Nature* **518**, 179 (2015).

[2] C. Proust and L. Taillefer, *Annual Review of Condensed Matter Physics* **10**, 409 (2019).

[3] P. W. Anderson, *Science* **235**, 1196 (1987).

TABLE I. Summary of the quantum phases for the t - t' - J and σt - t' - J model on the 6-leg cylinder with doping ratio $\delta = 1/12$. The decay exponents of correlation functions are presented at $t'/t = -0.1, 0, 0.2$. The pairing correlation $P_{yy}(r)$ and single-particle Green's function $G(r)$ have been defined in the text. Here we also show the decay exponents of the density correlation function $D(r) = \langle \hat{n}(x, y) \hat{n}(x+r, y) \rangle - \langle \hat{n}(x, y) \rangle \langle \hat{n}(x+r, y) \rangle$ and spin correlation function $F(r) = \langle \mathbf{S}(x, y) \cdot \mathbf{S}(x+r, y) \rangle$. The correlation length of exponential fitting is denoted as ξ , and the power exponent of algebraic fitting is denoted by K . The fitted correlation functions for the t - t' - J and σt - t' - J models are obtained by keeping 12000 SU(2) multiplets and 15000 U(1) states, respectively. For the FL-like phase in the σt - t' - J model, the pairing correlation $P_{yy}(r)$ will behave as a product of two Green's functions and thus also follows an algebraic decay, as shown in Fig. 4(d). Nonetheless, this algebraic decay does not characterize a quasi-long-range SC order. Therefore, we do not fit the power exponent K_{sc} in the FL-like phase.

| Models | Parameters | Phase | $P_{yy}(r)$ | $D(r)$ | $G(r)$ | $F(r)$ |
|-------------------------|---------------|----------|-------------------------|----------------------|----------------------|----------------------|
| t - t' - J | $t'/t = -0.1$ | CDW | $\xi_{sc} \approx 3.02$ | $\xi_c \approx 4.72$ | $\xi_G \approx 2.73$ | $\xi_s \approx 5.91$ |
| | $t'/t = 0$ | CDW | $\xi_{sc} \approx 2.95$ | $\xi_c \approx 4.96$ | $\xi_G \approx 2.03$ | $\xi_s \approx 6.13$ |
| | $t'/t = 0.2$ | SC + CDW | $K_{sc} \approx 0.55$ | $K_c \approx 1.56$ | $\xi_G \approx 1.97$ | $\xi_s \approx 3.32$ |
| σt - t' - J | $t'/t = -0.1$ | FL-like | — | $K_c \approx 1.93$ | $K_G \approx 0.96$ | $K_s \approx 1.83$ |
| | $t'/t = 0$ | FL-like | — | $K_c \approx 1.55$ | $K_G \approx 0.81$ | $K_s \approx 1.69$ |
| | $t'/t = 0.2$ | FL-like | — | $K_c \approx 1.82$ | $K_G \approx 0.94$ | $K_s \approx 1.95$ |

- [4] P. W. Anderson, P. A. Lee, M. Randeria, T. M. Rice, N. Trivedi, and F. C. Zhang, *Journal of Physics: Condensed Matter* **16**, R755 (2004).
- [5] P. A. Lee, N. Nagaosa, and X.-G. Wen, *Rev. Mod. Phys.* **78**, 17 (2006).
- [6] Z. Y. Weng, *Int. J. Mod. Phys. B* **21**, 773 (2007).
- [7] M. Ogata and H. Fukuyama, *Rep. Prog. Phys.* **71**, 036501 (2008).
- [8] D. P. Arovas, E. Berg, S. A. Kivelson, and S. Raghu, *Annual Review of Condensed Matter Physics* **13**, 239 (2022).
- [9] S. R. White and D. J. Scalapino, *Phys. Rev. Lett.* **80**, 1272 (1998).
- [10] S. R. White and D. J. Scalapino, *Phys. Rev. B* **60**, R753 (1999).
- [11] S. R. White and D. J. Scalapino, *Phys. Rev. Lett.* **91**, 136403 (2003).
- [12] G. Hager, G. Wellein, E. Jeckelmann, and H. Fehske, *Phys. Rev. B* **71**, 075108 (2005).
- [13] P. Corboz, T. M. Rice, and M. Troyer, *Phys. Rev. Lett.* **113**, 046402 (2014).
- [14] J. P. F. LeBlanc, A. E. Antipov, F. Becca, I. W. Bulik, G. K.-L. Chan, C.-M. Chung, Y. Deng, M. Ferrero, T. M. Henderson, C. A. Jiménez-Hoyos, E. Kozik, X.-W. Liu, A. J. Millis, N. V. Prokof'ev, M. Qin, G. E. Scuseria, H. Shi, B. V. Svistunov, L. F. Tocchio, I. S. Tupitsyn, S. R. White, S. Zhang, B.-X. Zheng, Z. Zhu, and E. Gull (Simons Collaboration on the Many-Electron Problem), *Phys. Rev. X* **5**, 041041 (2015).
- [15] G. Ehlers, S. R. White, and R. M. Noack, *Phys. Rev. B* **95**, 125125 (2017).
- [16] B.-X. Zheng, C.-M. Chung, P. Corboz, G. Ehlers, M.-P. Qin, R. M. Noack, H. Shi, S. R. White, S. Zhang, and G. K.-L. Chan, *Science* **358**, 1155 (2017).
- [17] E. W. Huang, C. B. Mendl, S. Liu, S. Johnston, H.-C. Jiang, B. Moritz, and T. P. Devereaux, *Science* **358**, 1161 (2017).
- [18] K. Ido, T. Ohgoe, and M. Imada, *Phys. Rev. B* **97**, 045138 (2018).
- [19] H.-C. Jiang, Z.-Y. Weng, and S. A. Kivelson, *Phys. Rev. B* **98**, 140505 (2018).
- [20] B. Ponsioen, S. S. Chung, and P. Corboz, *Phys. Rev. B* **100**, 195141 (2019).
- [21] M. Qin, C.-M. Chung, H. Shi, E. Vitali, C. Hubig, U. Schollwöck, S. R. White, and S. Zhang (Simons Collaboration on the Many-Electron Problem), *Phys. Rev. X* **10**, 031016 (2020).
- [22] M. Qin, T. Schäfer, S. Andergassen, P. Corboz, and E. Gull, *Annual Review of Condensed Matter Physics* **13**, 275 (2022).
- [23] H. Xu, H. Shi, E. Vitali, M. Qin, and S. Zhang, *Phys. Rev. Research* **4**, 013239 (2022).
- [24] G. B. Martins, J. C. Xavier, L. Arrachea, and E. Dagotto, *Phys. Rev. B* **64**, 180513 (2001).
- [25] S. Sorella, G. B. Martins, F. Becca, C. Gazza, L. Capriotti, A. Parola, and E. Dagotto, *Phys. Rev. Lett.* **88**, 117002 (2002).
- [26] C. T. Shih, T. K. Lee, R. Eder, C.-Y. Mou, and Y. C. Chen, *Phys. Rev. Lett.* **92**, 227002 (2004).
- [27] S. R. White and D. J. Scalapino, *Phys. Rev. B* **79**, 220504 (2009).
- [28] A. Eberlein and W. Metzner, *Phys. Rev. B* **89**, 035126 (2014).
- [29] J. F. Dodaro, H.-C. Jiang, and S. A. Kivelson, *Phys. Rev. B* **95**, 155116 (2017).
- [30] H.-C. Jiang and T. P. Devereaux, *Science* **365**, 1424 (2019).
- [31] C.-M. Chung, M. Qin, S. Zhang, U. Schollwöck, and S. R. White (The Simons Collaboration on the Many-Electron Problem), *Phys. Rev. B* **102**, 041106 (2020).
- [32] Y.-F. Jiang, J. Zaanen, T. P. Devereaux, and H.-C. Jiang, *Phys. Rev. Research* **2**, 033073 (2020).
- [33] X. Lu, D.-W. Qu, Y. Qi, W. Li, and S.-S. Gong, *Phys. Rev. B* **107**, 125114 (2023).
- [34] S. Jiang, D. J. Scalapino, and S. R. White, *Phys. Rev. B* **106**, 174507 (2022).
- [35] S. Jiang, D. J. Scalapino, and S. R. White, *Proceedings of the National Academy of Sciences* **118**, e2109978118 (2021).
- [36] H.-C. Jiang and S. A. Kivelson, *Phys. Rev. Lett.* **127**, 097002 (2021).
- [37] S. Gong, W. Zhu, and D. N. Sheng, *Phys. Rev. Lett.* **127**, 097003 (2021).
- [38] H.-C. Jiang, S. A. Kivelson, and D.-H. Lee, (2023), [arXiv:2302.11633](https://arxiv.org/abs/2302.11633).
- [39] A. Wietek, *Phys. Rev. Lett.* **129**, 177001 (2022).
- [40] A. Wietek, Y.-Y. He, S. R. White, A. Georges, and E. M. Stoudenmire, *Phys. Rev. X* **11**, 031007 (2021).
- [41] D.-W. Qu, B.-B. Chen, X. Lu, Q. Li, Y. Qi, S.-S. Gong, W. Li, and G. Su, (2022), [arXiv:2211.06322](https://arxiv.org/abs/2211.06322).
- [42] S. Jiang, D. J. Scalapino, and S. R. White, (2023), [arXiv:2303.00756](https://arxiv.org/abs/2303.00756).
- [43] H. Xu, C.-M. Chung, M. Qin, U. Schollwöck, S. R. White, and S. Zhang, (2023), [arXiv:2303.08376](https://arxiv.org/abs/2303.08376).
- [44] A. Luther and V. J. Emery, *Phys. Rev. Lett.* **33**, 589 (1974).

- [45] L. Balents and M. P. A. Fisher, [Phys. Rev. B **53**, 12133 \(1996\)](#).
- [46] C. Kim, P. J. White, Z.-X. Shen, T. Tohyama, Y. Shibata, S. Maekawa, B. O. Wells, Y. J. Kim, R. J. Birgeneau, and M. A. Kastner, [Phys. Rev. Lett. **80**, 4245 \(1998\)](#).
- [47] E. Pavarini, I. Dasgupta, T. Saha-Dasgupta, O. Jepsen, and O. K. Andersen, [Phys. Rev. Lett. **87**, 047003 \(2001\)](#).
- [48] K. Tanaka, T. Yoshida, A. Fujimori, D. H. Lu, Z.-X. Shen, X.-J. Zhou, H. Eisaki, Z. Hussain, S. Uchida, Y. Aiura, K. Ono, T. Sugaya, T. Mizuno, and I. Terasaki, [Phys. Rev. B **70**, 092503 \(2004\)](#).
- [49] D. N. Sheng, Y. C. Chen, and Z. Y. Weng, [Phys. Rev. Lett. **77**, 5102 \(1996\)](#).
- [50] Z. Y. Weng, D. N. Sheng, Y.-C. Chen, and C. S. Ting, [Phys. Rev. B **55**, 3894 \(1997\)](#).
- [51] K. Wu, Z. Y. Weng, and J. Zaanen, [Phys. Rev. B **77**, 155102 \(2008\)](#).
- [52] H.-C. Jiang, S. Chen, and Z.-Y. Weng, [Phys. Rev. B **102**, 104512 \(2020\)](#).
- [53] See supplementary materials for more supporting data.
- [54] S. R. White, [Phys. Rev. Lett. **69**, 2863 \(1992\)](#).
- [55] I. P. McCulloch and M. Gulácsi, [Europhysics Letters \(EPL\) **57**, 852 \(2002\)](#).
- [56] Y. Huang, S.-S. Gong, and D. N. Sheng, (2022), [arXiv:2209.00833](#).
- [57] J.-Y. Zhao, S. A. Chen, H.-K. Zhang, and Z.-Y. Weng, [Phys. Rev. X **12**, 011062 \(2022\)](#).
- [58] S. Chen, Z. Zhu, and Z.-Y. Weng, Two-hole ground state wavefunction: Non-BCS pairing in a t - J two-leg ladder, [Phys. Rev. B **98**, 245138 \(2018\)](#).
- [59] Z. Zhu, D. N. Sheng, and Z.-Y. Weng, [Phys. Rev. B **98**, 035129 \(2018\)](#).
- [60] J.-Y. Zhao, S. A. Chen, R.-Y. Sun, and Z.-Y. Weng, (2022), [arXiv:2210.04918](#).
- [61] J.-X. Zhang and Z.-Y. Weng, (2022), [arXiv:2208.10519](#).

Supplementary Materials for: “Sign structure in the square-lattice t - t' - J model and numerical consequences”

In the supplementary materials, we provide more analytical and numerical results to support the conclusions presented in the main text. In Sec. I, we give a detailed derivation of the precise sign structure of the t - t' - J model, in which the phase-string sign structure, in addition to the conventional Fermi statistics between the doped holes and the geometric Berry phase due to the sign of t'/t , will be identified, together with the analytic expression of the positive weight function. Furthermore, we also present an alternative derivation of the sign structure and demonstrate its applicability to non-bipartite lattices, such as triangular lattices or systems with the next-nearest-neighbor (NNN) superexchange interactions. In Sec. II, we show more density matrix renormalization group (DMRG) simulation results for the binding energy, including the 5-leg t - t' - J model and the extrapolations of the ground-state energies in different sectors versus bond dimension for the 6-leg t - t' - J model. In Sec. III, we present the DMRG measurement results for the 5-leg t - t' - J model. In Sec. IV, we show more DMRG results of the electron densities in momentum space.

I. The exact sign structure of the t - t' - J Hamiltonian

In this section, we give a rigorous proof of the partition function in Eq. (2) and the sign structure given in Eq. (4). We shall start with the slave-fermion formalism, in which the electron operator is defined as $c_{i\sigma} = f_i^\dagger b_{i\sigma}$, with f_i^\dagger denoting the fermionic holon operator and $b_{i\sigma}$ denoting the bosonic spinon operator, which satisfies the constraint $f_i^\dagger f_i + \sum_\sigma b_{i\sigma}^\dagger b_{i\sigma} = 1$. To clarify the sign structure of this model, we explicitly incorporate the Marshall sign into the S_z -spin representation by implementing the substitution

$$b_{i\sigma} \rightarrow (-\sigma)^i b_{i\sigma} \quad (\text{S1})$$

such that

$$c_{i\sigma} = (-\sigma)^i f_i^\dagger b_{i\sigma}. \quad (\text{S2})$$

Then, the t - t' - J model can be expressed under this transformation as follows:

$$H_{t-t'-J} = -t(P_{o\uparrow} - P_{o\downarrow}) - t'T_o - \frac{J}{4}(Q + P_{\uparrow\downarrow}), \quad (\text{S3})$$

where

$$P_{o\sigma} = \sum_{\langle ij \rangle} b_{i\sigma}^\dagger b_{j\sigma} f_j^\dagger f_i + \text{h.c.} \quad (\text{S4})$$

$$T_o = \sum_{\langle\langle ij \rangle\rangle\sigma} b_{i\sigma}^\dagger b_{j\sigma} f_j^\dagger f_i + \text{h.c.} \quad (\text{S5})$$

$$P_{\uparrow\downarrow} = \sum_{\langle ij \rangle} b_{i\uparrow}^\dagger b_{j\downarrow}^\dagger b_{i\downarrow} b_{j\uparrow} + \text{h.c.} \quad (\text{S6})$$

$$Q = \sum_{\langle ij \rangle} (n_{i\uparrow} n_{j\downarrow} + n_{i\downarrow} n_{j\uparrow}). \quad (\text{S7})$$

Here $P_{o\sigma}(T_o)$ denotes the hole-spin NN (NNN) exchange operator, $P_{\uparrow\downarrow}$ the NN spin superexchange operator, and Q describes a potential term between NN spins. By making the high-temperature series expansion [cf. Eq. (3)] of the partition function up to all orders [51]

$$\begin{aligned} Z_{t-t'-J} &= \text{Tr} e^{-\beta H_{t-t'-J}} = \text{Tr} \sum_{n=0}^{\infty} \frac{\beta^n}{n!} (-H_{t-t'-J})^n \\ &= \sum_{n=0}^{\infty} \frac{(J\beta/4)^n}{n!} \text{Tr} \left[\sum \dots \left(\frac{4t}{J} P_{o\uparrow} \right) \dots P_{\uparrow\downarrow} \dots \left(\frac{-4t}{J} P_{o\downarrow} \right) \dots \left(\frac{4t'}{J} T_o \right) \dots Q \dots \right]_n \\ &= \sum_{n=0}^{\infty} (-1)^{N_{\uparrow}^h} (\text{sgn } t')^{N_{\uparrow}^h} \frac{(J\beta/4)^n}{n!} \text{Tr} \left[\sum \dots \left(\frac{4t}{J} P_{o\uparrow} \right) \dots P_{\uparrow\downarrow} \dots \left(\frac{4t}{J} P_{o\downarrow} \right) \dots \left(\frac{4|t'|}{J} T_o \right) \dots Q \dots \right]_n \quad (\text{S8}) \end{aligned}$$

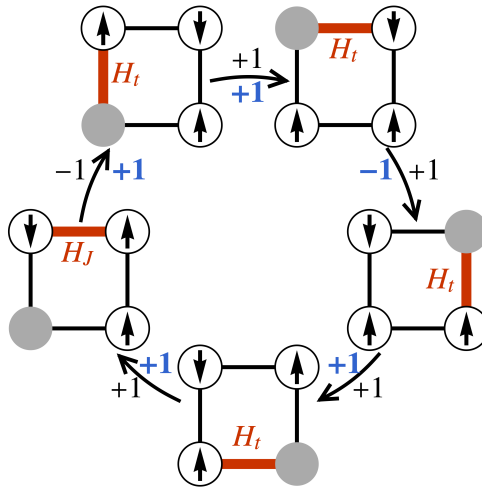


FIG. S1. Illustration of an example of a closed loop for the doped square lattice, with matrix elements of the interaction process ($-H$) labeled by thick red lines. The black (gray) ± 1 markers indicate the sign of the matrix elements before (after) the Marshall sign transformation Eq. (S2). Additionally, the grey circles represent holes.

where the NN hopping integral is assumed to always be positive for simplicity, that is $t > 0$. The notation $[\sum \dots]_n$ indicates the summation over all n -block production, and because of the trace, the initial and final hole and spin configurations should be the same such that all contributions to $Z_{t-t'-J}$ can be characterized by closed loops of holes and spins. Here N_{\downarrow}^h denotes the number of NN exchanges between down-spins and holes, as well as N_{\uparrow}^h denotes the number of NNN exchanges between spins and holes, regardless of spin direction. Inserting complete Ising basis with holes

$$\sum_{\phi\{l_h\}} |\phi; \{l_h\}\rangle \langle \phi; \{l_h\}| = 1 \quad (\text{S9})$$

between the operator inside the trace with ϕ specifying the spin configuration and $\{l_h\}$ denoting the positions of holes. Then, all the elements inside the trace are positive and the partition function can arrive at a compact expression:

$$Z_{t-t'-J} = \sum_C \tau_C W_{t-t'-J}[C], \quad (\text{S10})$$

where all the sign information is captured by

$$\tau_C \equiv \tau_C^0 \times (-1)^{N_{\downarrow}^h}, \quad (\text{S11})$$

with

$$\tau_C^0 \equiv (-1)^{N_{\text{ex}}^h} \times [\text{sgn}(t')]^{N_{\uparrow}^h}, \quad (\text{S12})$$

which is consistent with Eq. (4) in the main text. Here, N_{ex}^h denotes the number of exchanges between holes due to fermionic statistics of holon f . Such a sign structure is precisely described at arbitrary doping, temperature, and finite-size for $t-t'-J$ model, which has been previously identified at $t' = 0$ in Ref. 51. In addition, the non-negative weight $W[C]$ for closed loop C is given by:

$$W_{t-t'-J}[C] = \left(\frac{4t}{J}\right)^{M_t[C]} \left(\frac{4|t'|}{J}\right)^{M_{t'}[C]} \sum_n \frac{(J\beta/4)^n}{n!} \delta_{n, M_t + M_{t'} + M_{\uparrow\downarrow} + M_Q} \geq 0, \quad (\text{S13})$$

in which M_t and $M_{t'}$ represent the total steps of the hole NN and NNN ‘‘hoppings’’ along the closed loops for a given path C with length n , respectively. Also, $M_{\uparrow\downarrow}$ represents the steps of NN spin exchange process, while M_Q represents the total number of down spins interacting with up spins via the S_z components of the superexchange term.

In summary, the sign structure of the $t-t'-J$ model comprises not only the effects of NNN hopping and the traditional fermionic statistics encoded in τ_C^0 , but also a significant component of $(-1)^{N_{\downarrow}^h}$ originating from the NN hole hopping process. This

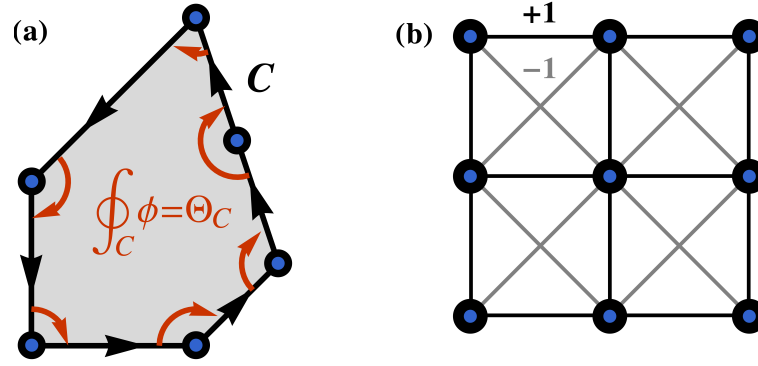


FIG. S2. (a) Illustration the geometric phase ϕ_{ij} , where the red arrow indicates the non-zero contribution of the points on the selected closed loop (black line), with the total inner angle sum denoted as Θ_C . (b) In the t - t' - J model, one possible gauge choice for ϕ_{ij} is shown here, with black bonds representing nearest-neighbor (NN) links having $e^{i\phi_{ij}} = +1$ and gray bonds representing next-nearest-neighbor (NNN) links having $e^{i\phi_{ij}} = -1$.

component is depicted in Fig. S1(a) by blue ± 1 on the arrows. From the viewpoint of the original representation, i.e., before the Marshall sign transformation in Eq. (S2), each spin flip results in a negative sign under the Ising basis, since $\langle \downarrow_i \uparrow_j | JS_i^- S_j^+ | \uparrow_i \downarrow_j \rangle > 0$. Therefore, in the presence of hole hopping, an odd number of spin flips can occur in the closed loop of a bipartite lattice, as illustrated in Fig. S1(a) by black ± 1 on the arrows.

Furthermore, by introducing the σt - t' - J model, in which the original kinetic energy term Eq.(1) is replaced by:

$$H_{\sigma t-t'} = -\sigma t \sum_{\langle ij \rangle} c_{i,\sigma}^\dagger c_{j,\sigma} - t' \sum_{\langle\langle ij \rangle\rangle} c_{i,\sigma}^\dagger c_{j,\sigma} + \text{h.c.}, \quad (\text{S14})$$

where an extra spin dependent sign σ is inserted into the NN hopping term that cancels the “-” sign in front of the $P_{o\downarrow}$. Consequently, σt - t' - J model under the representation of Eq. (S2) can be rewritten as:

$$H_{\sigma t-t'-J} = -t(P_{o\uparrow} + P_{o\downarrow}) - t'T_o - \frac{J}{4}(Q + P_{\uparrow\downarrow}), \quad (\text{S15})$$

with the partition function under the high-temperature series expansion:

$$Z_{\sigma t-t'-J} = \sum_{n=0}^{\infty} (\text{sgn } t')^{N_{t'}} \frac{(J\beta/4)^n}{n!} \text{Tr} \left[\sum \dots \left(\frac{4t}{J} P_{o\uparrow} \right) \dots P_{\uparrow\downarrow} \dots \left(\frac{4t}{J} P_{o\downarrow} \right) \dots \left(\frac{4|t'|}{J} T_o \right) \dots Q \dots \right]_n. \quad (\text{S16})$$

Consequently, the sign structure for σt - t' - J model is given by:

$$\tau_C^{\sigma t-t'-J} = \tau_C^0, \quad (\text{S17})$$

where τ_C^0 is given by Eq. (S12) and the positive weight $W[C]$ for each path remains unchanged, leading to Eq. (6).

Extension of exact sign structure to non-bipartite lattices

We have established a rigorous proof of the exact sign structure for the t - t' - J model. In this subsection, we provide an alternative derivation of the sign structure and demonstrate its applicability to non-bipartite lattices, such as triangular lattices or systems with next-nearest-neighbor (NNN) superexchange interactions.

Here we use the extended t - J model on an *arbitrary* lattice as an example, with the Hamiltonian given by

$$H = -T \sum_{ij,\sigma} c_{i\sigma}^\dagger c_{j\sigma} + \text{h.c.} + K \sum_{ij} \left(\mathbf{S}_i \cdot \mathbf{S}_j - \frac{1}{4} n_i n_j \right). \quad (\text{S18})$$

Unlike the main text, where the sum indexes $\langle ij \rangle$ represent only the NN links, here the sum includes all allowed links that can connect any two sites. To begin, instead of applying the Marshall basis transformation as described in Eq. (S1), which relies on the A - B sublattice division, we propose a redefinition of the up-spinon operator as follows:

$$b_{i\uparrow} \rightarrow b_{i\uparrow} e^{-i\Phi_i} \quad (\text{S19})$$

while keeping the down-spinon operator unchanged, such that

$$\begin{aligned} c_{i\uparrow} &= f_i^\dagger b_{i\uparrow} e^{-i\Phi_i} \\ c_{i\downarrow} &= f_i^\dagger b_{i\downarrow}, \end{aligned} \quad (\text{S20})$$

where

$$\Phi_i \equiv \sum_{l \neq i} \theta_i(l) = \sum_{l \neq i} \text{Im} \ln(z_i - z_l), \quad (\text{S21})$$

with z_i as the complex coordinate at site i . Hence, by simply using the relations $\theta_i(j) - \theta_j(i) = \pm\pi$, the extended t - J model in become:

$$\begin{aligned} H_{t-t'} &= - \sum_{ij,\sigma} \sigma T b_{i\sigma}^\dagger b_{j\sigma} f_j^\dagger f_i e^{\frac{i(\sigma+1)}{2} \phi_{ij}} + h.c. \\ &\quad - \frac{K}{4} \sum_{\langle ij \rangle \sigma} \left(n_{i\sigma} n_{j-\sigma} + b_{i\sigma}^\dagger b_{j-\sigma}^\dagger b_{i-\sigma} b_{j\sigma} e^{i\sigma \phi_{ij}} \right), \end{aligned} \quad (\text{S22})$$

where

$$\phi_{ij} = \sum_{l \neq ij} [\theta_i(l) - \theta_j(l)] \quad (\text{S23})$$

acting like a gauge potential with a gauge invariant strength given by $\sum_C \phi_{ij} = \Theta_C$ for a closed loop C on the lattice. The symbol Θ_C denotes the interior angle sum of the closed-loop C depicted in Fig. S2(a). It is evident that any point that is situated outside or inside the loop contributes 0 or $\pm 2\pi$ to Θ_C , respectively. Only the sites l on the closed loop C contribute nontrivial values to the interior angle, such that the sum of interior angles over all the points $l \in C$ corresponds to the total contribution, as illustrated in Fig. S2(a). Importantly, the phase ϕ_{ij} presented here is universally applicable to arbitrary lattices, irrespective of whether they are bipartite or not. Notably, for a bipartite system such as the t - J model on a square lattice with $t' = 0$, Θ_C is equal to $2\pi\mathbb{Z}$ for any closed loop, and the phase ϕ_{ij} can be completely gauged away.

As the result, in Eq. (S22), the hidden sign structure of extended t - J model on an arbitrary lattice is explicitly decomposed into the geometry phase ϕ_{ij} and the extra σ -sign in the hopping term, which is commonly referred to as the ‘‘phase string effect’’. To derive the sign structure Eq. (S11) of t - t' - J model on a square lattice, a proper gauge can be selected, as shown in Fig. S2(b), where NN links with $e^{i\phi_{ij}} = +1$ and NNN links with $e^{i\phi_{ij}} = -1$, to combine these two components of frustration, yielding Eq. (S11).

II. More DMRG data for the binding energy

In the main text, we have shown the system length L_x dependence of binding energies for the 4-leg σt - t' - J model at $\delta = 1/12$. Here, we present the same data for $\delta = 1/8$ in Fig. S3(a), supporting the absent binding energies of the σt - t' - J model in the infinite- L_x limit shown in Fig. 2(b) of the main text.

We have also computed the binding energies for the odd-leg t - t' - J model, including $L_y = 3$ and $L_y = 5$. For 3-leg systems, we obtain the almost vanished binding energies. However, on the wider 5-leg systems, the binding energies are negative [Figs. S3(b) and S3(c)], consistent with hole pairing and indicating that the hole pairing exists on both even- and odd-leg t - t' - J model at finite doping. In contrast, for the 5-leg σt - t' - J model, our DMRG calculations also find very small positive binding energies on the finite- L_x cylinder (not shown here), similar to the 6-leg results demonstrated in Fig. 2(d) of the main text, which consistently indicates the absence of hole binding in the σt - t' - J model.

For calculating the binding energy on the 4-leg systems, we can obtain the fully converged energies. For the wider 5- and 6-leg t - t' - J model we need to carefully check the convergence of the energies in the three sectors $E(N_h, S)$. For this purpose, we obtain the energies $E(N_h, S)$ by keeping different bond dimensions, and extrapolate these energies to the infinite-bond-dimension limit. Then we compute the binding energy using the extrapolated results. In Fig. S4, we show the bond-dimension dependence of the obtained energies $E(N_h, S)$ for $t'/t = -0.1, 0, 0.2$ on the $L_x = 32, L_y = 6$ cylinder at $1/12$ doping. We keep the bond dimensions up to 10000 – 15000 SU(2) multiplets to ensure a good linear extrapolation behavior of the data. We implement the linear fitting $\mathcal{C}(1/D) = a/D + \mathcal{C}(0)$ to obtain the energy in the infinite-bond-dimension limit E_∞ , from which we calculate the binding energies shown in Fig. 2(d) of the main text. Notice that for 5-leg systems in Figs. S3(b) and S3(c), we do not show the binding energies at $t'/t = -0.2$ since the energy at the $S = 1$ sector for $\delta = 1/8$ does not exhibit a smooth dependence on bond dimension, which cannot give us an accurate extrapolation of the energy versus bond dimension.

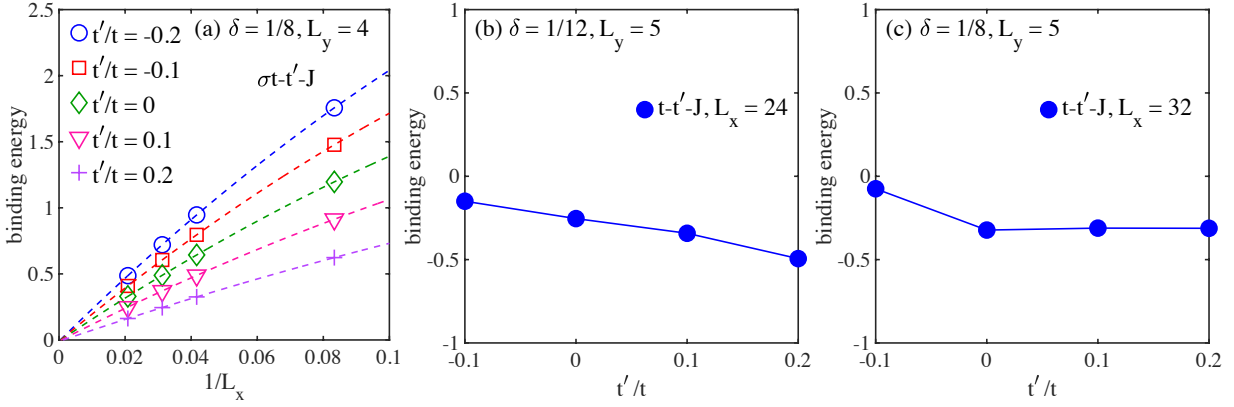


FIG. S3. Binding energy in the $t-t'-J$ and $\sigma t-t'-J$ models. (a) Extrapolations of binding energies versus system length for the 4-leg $\sigma t-t'-J$ model at $\delta = 1/8$. The binding energies are fitted by a second-order polynomial function $\mathcal{C}(1/L_x) = \mathcal{C}(0) + a/L_x + b/L_x^2$. (b) and (c) show the binding energies for the $t-t'-J$ model on the $L_y = 5, L_x = 24$ cylinder at $\delta = 1/12$ and the $L_y = 5, L_x = 32$ cylinder at $\delta = 1/8$, respectively. The binding energies are calculated using the energies $E(N_h, S)$ after the extrapolation to the infinite-bond-dimension limit.

For the $\sigma t-t'-J$ model on the 6-leg cylinder, we find that although the energies $E(N_h, S)$ get improved with increasing bond dimension, the binding energy is almost independent of bond dimension in our calculation. Therefore, we do not extrapolate the energies but use the results by keeping the largest bond dimension.

III. DMRG measurements for the 5-leg systems

In Fig. S3, we have shown the finite binding energies for the 5-leg $t-t'-J$ model. Here we present the corresponding pairing correlation $P_{yy}(r)$, charge density correlation $D(r)$, and charge density profile $n(x)$ in Fig. S5. For $t'/t = -0.1-0.2$, the pairing correlations can be fitted quite well as the algebraic decay with the power exponents $K_{sc} < 2$, indicating the quasi-long-range superconducting order and is consistent with the hole binding shown in Figs. S3(b) and S3(c). In particular, pairing correlations are enhanced with t'/t increasing from $t'/t < 0$ to $t'/t > 0$, which agrees with the findings on 4- and 6-leg systems and implies that the positive t'/t can enhance the coherence of paired holes should be common on both even- and odd-leg systems.

On the other hand, the charge density correlations also appear to decay algebraically with the power exponents $K_c < 2$, which is associated with weak charge density oscillations. These results indicate a weak charge density order coexisting with the quasi-long-range superconducting order in the studied parameter regime of the 5-leg $t-t'-J$ model.

IV. Electron momentum distribution

We have shown the electron momentum distributions $n(\mathbf{k}) = \frac{1}{N} \sum_{i,j,\sigma} \langle \hat{c}_{i,\sigma}^\dagger \hat{c}_{j,\sigma} \rangle e^{i\mathbf{k} \cdot (\mathbf{r}_i - \mathbf{r}_j)}$ for the 6-leg cylinder at $\delta = 1/12$ in the main text. Here, we supplement with similar results for $\delta = 1/8$ doping as shown in Fig. S6. In the $t-t'-J$ model, a large Fermi surface is visible, and the topology of Fermi surface shows difference in the CDW and SC phases. By contrast, in the $\sigma t-t'-J$ model, two small Fermi pockets appear at $\mathbf{k} = (\pi, \pi)$ and $\mathbf{k} = (0, 0)$, which have a weak t'/t dependence and are contributed from the spin-up propagator and spin-down propagator, respectively. Similarly, on the 5-leg $t-t'-J$ model, the topology of Fermi surface for $t'/t < 0$ and $t'/t > 0$ are distinct, as shown in Fig. S7, which is analogous to the observations on 6-leg systems [Figs. S6(a) and S6(b)]. We also present the results for the 4-leg $\sigma t-t'-J$ model in Fig. S8, which show the consistent features with the results on the 6-leg cylinder.

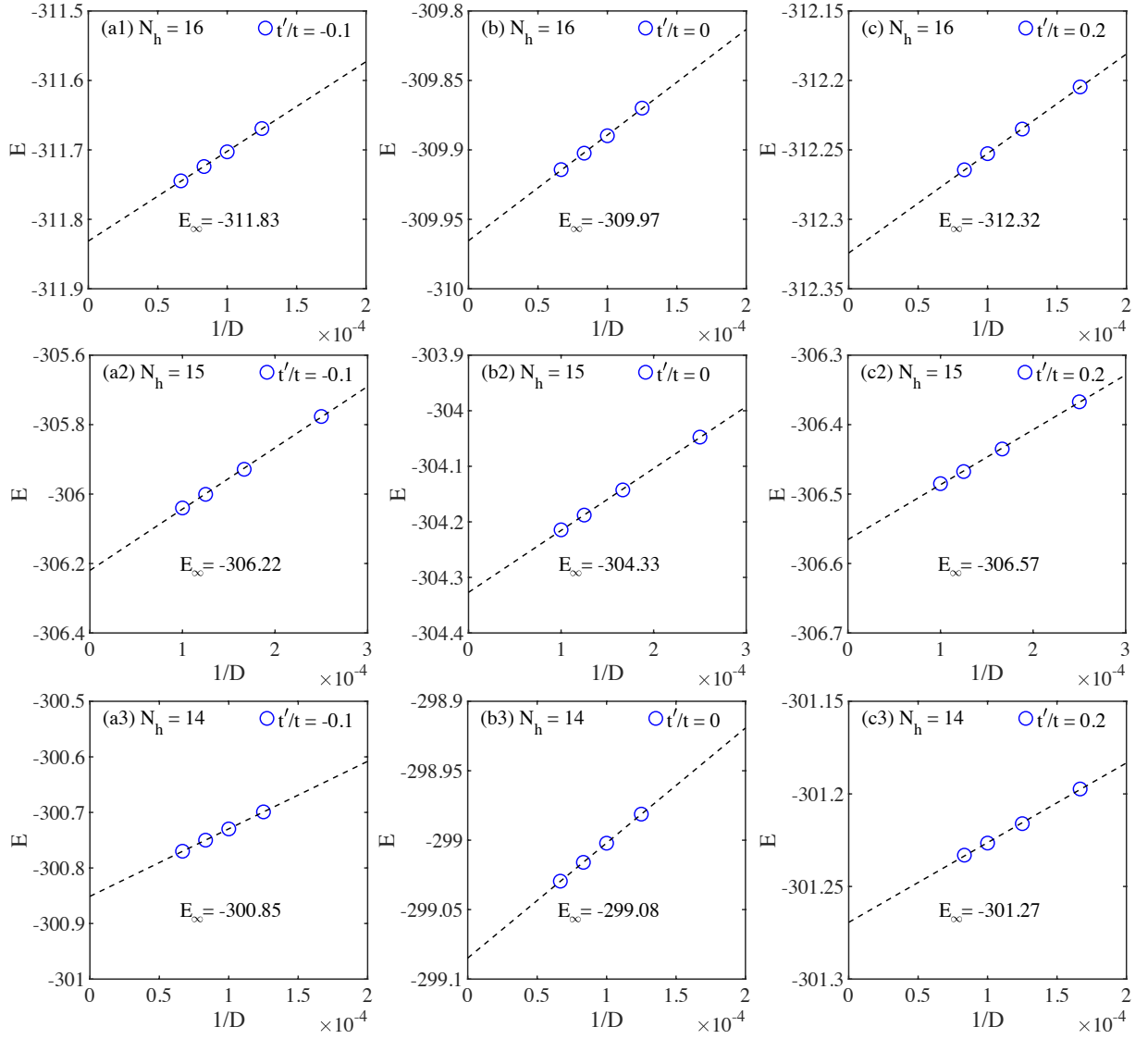


FIG. S4. Extrapolations of the ground-state energies $E(N_h, S)$ for the 6-leg t - t' - J model on the size $L_y \times L_x = 6 \times 32$. (a1-c1) show the bond dimension scaling of the ground-state energy at $t'/t = -0.1, 0$, and 0.2 with the hole number $N_h = 16$. (a2-c2) and (a3-c3) show the similar results for the hole numbers $N_h = 15$ and $N_h = 14$, respectively. We keep the bond dimensions D up to 10000 – 15000 $SU(2)$ multiplets. The energies are extrapolated by a linear function $\mathcal{C}(1/D) = a/D + \mathcal{C}(0)$ to give the energy E_∞ in the infinite bond dimension limit.

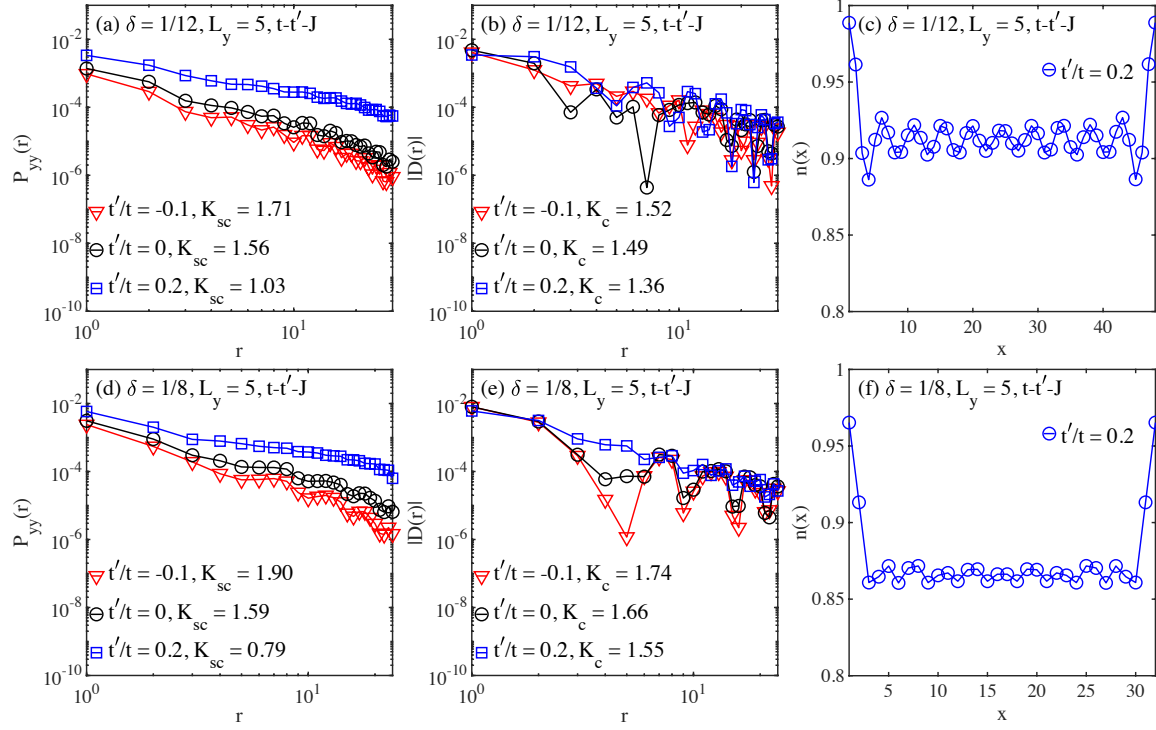


FIG. S5. Pairing correlation $P_{yy}(r)$, charge density correlation $D(r)$ and charge density profile $n(x)$ on the 5-leg $t-t'-J$ model. (a) and (b) show the pairing correlation $P_{yy}(r)$ and density correlation $D(r)$, respectively, for different t'/t on the $L_x = 48$ cylinder with $\delta = 1/12$. (c) Charge density profile $n(x)$ for $t'/t = 0.2$ on the $L_x = 48$ cylinder with $\delta = 1/12$. (d)-(f) are the similar plots on the $L_x = 32$ cylinder with $\delta = 1/8$. Here, we keep 10000 SU(2) multiplets to obtain the results. K_{sc} and K_c are obtained by algebraic fitting of corresponding correlation function.

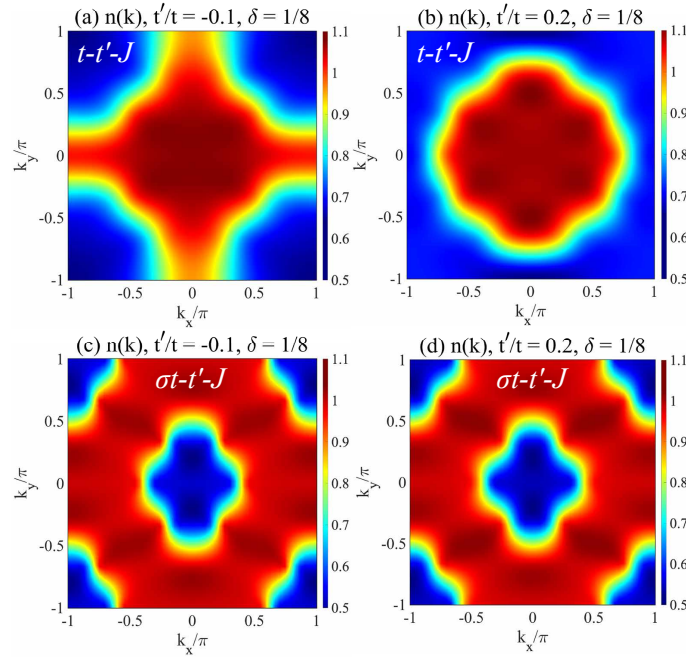


FIG. S6. Electron momentum distribution $n(\mathbf{k})$. (a) and (b) show the results of the $t-t'-J$ model, where an open and closed Fermi surface emerge in the CDW and SC phases. (c) and (d) show the results of the $\sigma t-t'-J$ model, where the electrons of spin-up and spin-down in $n(\mathbf{k})$ are displaced by (π, π) . Here $L_y = 6$, $t'/t = -0.1$ and 0.2 at the doping level $\delta = 1/8$.

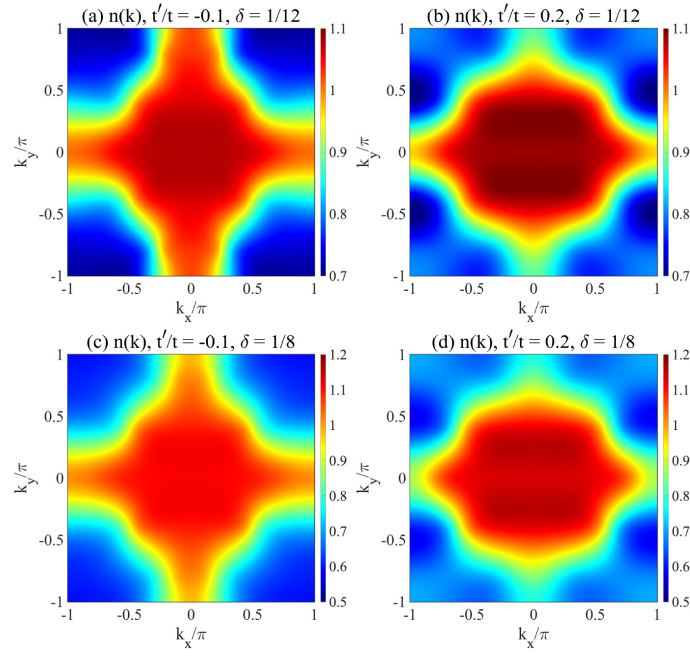


FIG. S7. Electron momentum distribution $n(\mathbf{k})$. (a) and (b) show the results of the t - t' - J model at $\delta = 1/12$. (c) and (d) show the similar results at $\delta = 1/8$. Here $L_y = 5$, $t'/t = -0.1$ and 0.2 .

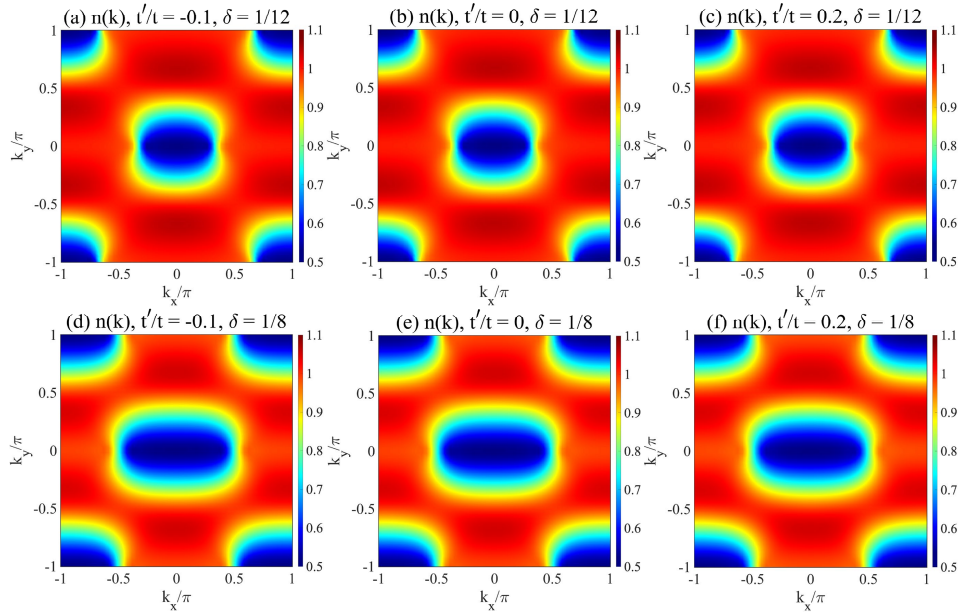


FIG. S8. Electron momentum distribution $n(\mathbf{k})$. (a-c) show the results of the σt - t' - J model at $\delta = 1/12$. (d-f) show the similar results at $\delta = 1/8$. The electrons of spin-up and spin-down in $n(\mathbf{k})$ are displaced by (π, π) . Here $L_y = 4$ and $t'/t = -0.1, 0, 0.2$.